Journal of Computational Mathematics, Vol.19, No.1, 2001, 41–54.

ANALYSIS OF MOVING MESH METHODS BASED ON GEOMETRICAL VARIABLES*[1)]

Tao Tang Wei-min Xue
(*Department of Mathematics, The Hong Kong Baptist University, Kowloon, Hong Kong*)

Ping-wen Zhang
(*School of Mathematics, Peking University, Beijing 100871, China*)

Dedicated to the 80th birthday of Professor Feng Kang

Abstract

In this study we will consider moving mesh methods for solving one-dimensional time dependent PDEs. The solution and mesh are obtained simultaneously by solving a system of *differential-algebraic* equations. The differential equations involve the solution and the mesh, while the algebraic equations involve several geometrical variables such as θ (the tangent angle), U (the normal velocity of the solution curve) and T (tangent velocity). The equal-arclength principle is employed to give a close form for T. For viscous conservation laws, we prove rigorously that the proposed system of moving mesh equations is well-posed, in the sense that first order perturbations for the solution and mesh can be controlled by the initial perturbation. Several test problems are considered and numerical experiments for the moving mesh equations are performed. The numerical results suggest that the proposed system of moving mesh equations is appropriate for solving (stiff) time dependent PDEs.

Key words: Moving mesh methods, Partial differential equations, Adaptive grids.

1. Introduction

Many methods have been proposed for adapting the mesh to achieve spatial resolution in the solution of partial differential equations. In addition to the capability of concentrating sufficient points about regions of rapid variation of the solution, a satisfactory mesh equation should be simple, easy to program, and reasonably insensitive to the choice of its adjustable parameters. The earliest work on adaptive techniques, based on moving finite element method (MFEM) was done by Miller [14, 12]. The gradient-weighted moving finite element (GWMFE) method was introduced recently by Miller as a geometrically motivated improvement over his earlier moving finite element methods. In [4, 5], Carlson and Miller reported on the design of the GWMFE codes and their extensive numerical trials on a variety of difficult PDEs and PDE systems. The *equidistribution principle*, first introduced by de Boor [7] for solving boundary value problems for ordinary differential equations, involves selecting mesh points such that some measure of the solution error is equalized over each subinterval. It has turned out to be an excellent principle for formulating moving mesh equations. In fact, a number of moving mesh methods have been

* Received November 27, 2000.

[1)]This research was supported by Hong Kong Baptist University, Hong Kong Research Grants Council, Special Funds for Major State Basic Research Projects of China and a Croucher Foundation Fellowship.

developed, and almost all are based at some point on an equidistribution principle, see, e.g., [1, 2, 9, 15, 17].

In this work, we present a new method for generating numerical grids. The main motivation of this research is from the fundamental work of Hou, Lowengrub and Shelley [10] in which a new formulation was proposed for computing the motion of fluid interfaces with surface tension. One of the key ideas in their paper involves using a geometrical frame of reference so that the tangent angle of the interface θ and its length L, rather than its x and y position are the dynamical variables. With the θ-L formulation, the corresponding numerical methods have no high-order time step stability constraints that are usually associated with surface tension. The equal-arclength principle of de Boor is also employed in [10]. This idea enables them to express a geometrical variable T (tangent velocity) entirely in terms of θ and L. The problems investigated in [10] are of periodic solutions and therefore the θ-L formulation is an appropriate setting. In fact, the θ-L approach is useful not only for problems with periodic solutions but also for problems with Neumann boundary conditions. However, for commonly used Dirichlet boundary conditions the θ-L formulation may not be well-posed due to the unspecified boundary conditions for θ. In this case, we propose to solve a system of parametrized differential equations for $x = x(\alpha, t)$ and $\tilde{u} = u(x(\alpha, t), t)$. A system of differential-algebraic equations (DAEs) will be obtained, which involve $x, \tilde{u}$ and some geometrical variables. This system, together with the given boundary conditions for x and $\tilde{u}$, will be solved numerically.

The paper is organized as follows. In §2, we introduce the differential-algebraic formulations based on geometrical variables. The well-posedness of the numerical approach will be briefly investigated in §3. Some detailed numerical procedures will be discussed in §4. Numerical experiments will be carried out in the final section.

2. The Formulation

We consider again a single time evolving PDE in 1-D

$$u_t = \mathcal{F}(x, u, t) \tag{2.1}$$

with appropriate boundary and initial conditions, where $\mathcal{F}$ is some nonlinear spatial differential operator. As described in [13], we convert equation (2.1) into the normal form

$$U = (x_t, u_t) \cdot \mathbf{n} = \frac{u_t}{\sqrt{1 + u_x^2}}. \tag{2.2}$$

Now u is allowed to be an evolving oriented 1-D *manifold* immersed in two dimensions. Implicit in this geometrical treatment is the assumption that a choice of the ratio between the horizontal and vertical scales has been made and fixed.

The motion of interface is reposed in terms of its tangent angle $\theta(\alpha, t)$ and its local arclength derivatives $\sigma(\alpha, t) = \sqrt{x_\alpha^2 + \tilde{u}_\alpha^2}$. Derivations have been given elsewhere (e.g. [10]), but for completeness it is included here. The tangent angle to the curve Γ, θ, is the angle between $\mathbf{s}$ and the x-axis. It satisfies

$$\mathbf{s}(\alpha, t) = \left(\frac{x_\alpha(x, t)}{\sigma(\alpha, t)}, \frac{\tilde{u}_\alpha(\alpha, t)}{\sigma(\alpha, t)} \right) = \big(\cos\theta(\alpha, t), \sin\theta(\alpha, t) \big). \tag{2.3}$$

The unit vector in the normal direction, $\mathbf{n}$, is perpendicular to $\mathbf{s}$ and satisfies

$$\mathbf{n}(\alpha, t) = \big(-\sin\theta(\alpha, t), \cos\theta(\alpha, t) \big). \tag{2.4}$$

The standard formula for θ is $\theta = \tan^{-1}(\tilde{u}_\alpha / x_\alpha)$. We can also construct θ from the *curvature* by using the formula $\theta_\alpha = \sigma\kappa$, where

$$\kappa = x_s u_{ss} - x_{ss} y_s = \big(x_\alpha \tilde{u}_{\alpha\alpha} - x_{\alpha\alpha}\tilde{u}_\alpha\big)/\sigma^3 .$$

In the above, s is arclength, but it is α and t that are the independent variables, and not s and t. Still, the α and s derivatives can be exchanged through the relation $\partial_s = \sigma^{-1}\partial_\alpha$.

We now turn to the derivations of the governing equations for σ and θ. Recall that the curve Γ evolves according to

$$\mathbf{X}_t = (x_t, \tilde{u}_t) = U\mathbf{n} + T\mathbf{s}. \tag{2.5}$$

It follows from (2.3)-(2.5) that

$$x_t = -U\sin\theta + T\cos\theta, \qquad \tilde{u}_t = U\cos\theta + T\sin\theta. \tag{2.6}$$

Using Frenet formulae $\partial_s \mathbf{s} = \kappa\mathbf{n}$ and $\partial_s \mathbf{n} = -\kappa\mathbf{s}$, together with $\theta_s = \kappa$ and $\partial_s = \sigma^{-1}\partial_\alpha$, we obtain the governing equations for σ and θ:

$$\sigma_t = T_\alpha - \theta_\alpha U\,, \qquad \theta_t = \frac{1}{\sigma}U_\alpha + \frac{T}{\sigma}\theta_\alpha\,. \tag{2.7}$$

We note that the shape of the curve is determined solely by its normal velocity U. A tangential motion gives only a change in frame for the parametrization of the curve. Therefore, a tangential velocity T may be introduced into the dynamics without altering the shape of the curve.

The equal-arclength principle. The general expression for T is now given based on the equal-arclength principle. In other words, we make $\sigma = \sqrt{x_\alpha^2 + \tilde{u}_\alpha^2}$ depended only upon t, and the PDE for σ in (2.7) reduces to an ODE. By requiring that σ is equal to its mean, we obtain

$$\sigma(\alpha, t) = \int_0^1 \sigma(\alpha', t)d\alpha' = L(t). \tag{2.8}$$

Under this requirement we can obtain a closed formula for T in terms of U and θ, where U is given by (2.2).

Equation for T. Differentiating (2.8) with respect to t and using the first equation in (2.7) yield

$$\begin{aligned} \sigma_t &= \int_0^1 \sigma_t(\alpha', t)d\alpha' = \int_0^1 \big(T_\alpha - \theta_\alpha U\big)d\alpha' \\ &= T(1,t) - T(0,t) - \int_0^1 \theta_\alpha U d\alpha'\,. \end{aligned} \tag{2.9}$$

This result, together with the first equation of (2.7), leads to

$$T_\alpha = T(1,t) - T(0,t) - \int_0^1 \theta_\alpha U d\alpha' + \theta_\alpha U.$$

Integrating the above equation from 0 to α gives

$$T(\alpha, t) = T(0,t) + \alpha\big(T(1,t) - T(0,t)\big) + \int_0^\alpha \theta_\alpha U d\alpha' - \alpha\int_0^1 \theta_\alpha U d\alpha'\,. \tag{2.10}$$

It remains to determine the boundary values for T. Since $x(0,t) \equiv a$ and $x(1,t) \equiv b$, where a, b are constants, we have $x_t(0,t) = x_t(1,t) = 0$. This, together with (2.6), lead to the boundary values for T:

$$T(0,t) = U(0,t)\tan\big(\theta(0,t)\big), \qquad T(1,t) = U(1,t)\tan\big(\theta(1,t)\big). \tag{2.11}$$

It is seen from (2.10) and (2.11) that T is expressed entirely in terms of U and θ.

Equation for L. Combining (2.8) and (2.9) gives the governing equation for L:

$$L'(t) = T(1,t) - T(0,t) - \int_0^1 \theta_\alpha U d\alpha'. \tag{2.12}$$

This, together with (2.11), suggests that L is determined entirely in terms of U and θ.

Equation for U. By the definition (2.2), $U = u_t(1+u_x^2)^{-1/2}$, we can express U in terms of $\tilde{u}, x, \theta$ and their derivatives. To see this, we use three examples to illustrate how to do this. The following formulas will be used frequently:

$$\begin{aligned}
&u_x = \tilde{u}_\alpha / x_\alpha\,, \qquad u_{xx} = \big(x_\alpha \tilde{u}_{\alpha\alpha} - x_{\alpha\alpha}\tilde{u}_\alpha\big)/x_\alpha^3\\
&u_x = \tan\theta\,, \qquad u_{xx} = \frac{\theta_\alpha}{\sigma\cos^3\theta}\\
&u_{xxx} = \big(x_\alpha \tilde{u}_{\alpha\alpha\alpha} - x_{\alpha\alpha\alpha}\tilde{u}_\alpha\big)/x_\alpha^5 - 3x_{\alpha\alpha}\big(x_\alpha\tilde{u}_{\alpha\alpha} - x_{\alpha\alpha}\tilde{u}_\alpha\big)/x_\alpha^5\\
&u_{xxx} = \frac{1}{\sigma^2\cos^4\theta}\big(\theta_{\alpha\alpha}\cos\theta + 3\,\theta_\alpha^2\sin\theta\big).
\end{aligned}$$

Example 2.1. Consider the Heat equation:

$$u_t = u_{xx} \qquad a < x < b, \quad 0 < t < T. \tag{2.13}$$

We then have the following formulas, one in terms of the physical variables x, u and another in terms of the geometrical variables θ, σ,

$$U = \frac{1}{x_\alpha^2\sigma}\big(x_\alpha u_{\alpha\alpha} - x_{\alpha\alpha}u_\alpha\big), \qquad U = \frac{\theta_\alpha}{\sigma\cos^2\theta}. \tag{2.14}$$

Example 2.2. For the viscous conservation laws

$$u_t + f(u)_x = \epsilon u_{xx}\,, \qquad \epsilon = Const. > 0 \tag{2.15}$$

we have the following formulas:

$$U = -\frac{1}{\sigma}f'(\tilde{u})\tilde{u}_\alpha + \frac{\epsilon}{x_\alpha^2\sigma}\big(x_\alpha\tilde{u}_{\alpha\alpha} - x_{\alpha\alpha}\tilde{u}_\alpha\big), \tag{2.16}$$

$$U = -f'(\tilde{u})\sin\theta + \frac{\epsilon\theta_\alpha}{\sigma\cos^2\theta}. \tag{2.17}$$

Example 2.3. Consider the one-dimensional KdV equation

$$u_t + \beta u u_x + \mu u_{xxx} = 0, \tag{2.18}$$

where β and μ are given constants. The following formulas held for the KdV equation:

$$U = \frac{-\beta}{\sigma}\tilde{u}\tilde{u}_\alpha - \frac{\mu}{\sigma}\big(x_\alpha\tilde{u}_{\alpha\alpha\alpha} - x_{\alpha\alpha\alpha}\tilde{u}_\alpha\big)/x_\alpha^3 + \frac{3\mu}{\sigma}x_{\alpha\alpha}\big(x_\alpha\tilde{u}_{\alpha\alpha} - x_{\alpha\alpha}\tilde{u}_\alpha\big)/x_\alpha^4 \tag{2.19}$$

$$U = -\beta\tilde{u}\sin\theta - \frac{\mu}{\sigma^2\cos^4\theta}\big(\theta_{\alpha\alpha}\cos\theta + 3\,\theta_\alpha^2\sin\theta\big). \tag{2.20}$$

As demonstrated in [10], an θ-L formulation provides simple and *uniform* differential system for problems with periodic solutions or Neumann boundary conditions. However, the θ-L formulation is not suitable for problems with Dirichlet boundary conditions, due to the unkown boundary values for θ. In this work, we propose to use an x-$\tilde{u}$ formulation to deal with the problems with Dirichlet boundary conditions. Let us consider Examples 2.1-2.3 to illustrate how to formulate the x-$\tilde{u}$ equations.

Heat equation. In this case, combining (2.6) and (2.14) gives

$$\begin{pmatrix} x \\ \tilde{u} \end{pmatrix}_t = \frac{1}{\sigma^2} \begin{pmatrix} \tan^2\theta & -\tan\theta \\ -\tan\theta & 1 \end{pmatrix} \begin{pmatrix} x \\ \tilde{u} \end{pmatrix}_{\alpha\alpha} + T \cdot \begin{pmatrix} \cos\theta \\ \sin\theta \end{pmatrix}. \tag{2.21}$$

The geometrical variables θ, σ and T are determined by the following constraints:

$$\theta = \tan^{-1}\left(u_\alpha / x_\alpha\right), \qquad \sigma = \sqrt{\tilde{u}_\alpha^2 + x_\alpha^2} \tag{2.22}$$

$$\begin{aligned} T = {} & U(0,t)\tan\left(\theta(0,t)\right) + \alpha\Big(U(1,t)\tan\left(\theta(1,t)\right) - U(0,t)\tan\left(\theta(0,t)\right)\Big) \\ & + \int_0^\alpha \theta_\alpha U d\alpha' - \alpha \int_0^1 \theta_\alpha U d\alpha' \end{aligned} \tag{2.23}$$

$$U = \frac{\theta_\alpha}{\sigma \cos^2\theta}. \tag{2.24}$$

In other words, we have obtained a system of differential-algebraic equations (DAEs), where the variables θ, U and T are constraints. This system, together with the given boundary conditions for x and $\tilde{u}$, can be solved numerically.

Viscous conservation laws. In this case, combining (2.6) and (2.17) gives

$$\begin{aligned} \begin{pmatrix} x \\ \tilde{u} \end{pmatrix}_t = {} & \frac{\epsilon}{\sigma^2} \begin{pmatrix} \tan^2\theta & -\tan\theta \\ -\tan\theta & 1 \end{pmatrix} \begin{pmatrix} x \\ \tilde{u} \end{pmatrix}_{\alpha\alpha} \\ & + f'(\tilde{u}) \sin\theta \begin{pmatrix} \sin\theta \\ -\cos\theta \end{pmatrix} + T \begin{pmatrix} \cos\theta \\ \sin\theta \end{pmatrix}. \end{aligned} \tag{2.25}$$

The above equations, together with (2.17) and (2.22)-(2.23), form a system of DAEs which can be solved numerically.

The KdV equation. In this case, combining (2.6) and (2.19) leads to

$$\begin{aligned} \begin{pmatrix} x \\ \tilde{u} \end{pmatrix}_t = {} & -\frac{\mu}{\sigma^3 \cos\theta} \begin{pmatrix} \tan^2\theta & -\tan\theta \\ -\tan\theta & 1 \end{pmatrix} \begin{pmatrix} x \\ \tilde{u} \end{pmatrix}_{\alpha\alpha\alpha} + \beta\tilde{u}\sin\theta \begin{pmatrix} \sin\theta \\ -\cos\theta \end{pmatrix} \\ & + \frac{3\mu}{\sigma^4} \frac{1}{\cos^2\theta} x_{\alpha\alpha} \begin{pmatrix} \tan^2\theta & -\tan\theta \\ -\tan\theta & 1 \end{pmatrix} \begin{pmatrix} x \\ \tilde{u} \end{pmatrix}_{\alpha\alpha} + T \begin{pmatrix} \cos\theta \\ \sin\theta \end{pmatrix}. \end{aligned} \tag{2.26}$$

The above equations, together with (2.20) and (2.22)-(2.23), again form a system of DAEs.

3. The Well-Posedness

In this section we consider the well-posedness of the adaptive grid method proposed in the last section. For simplicity, we only consider the viscous conservation laws (2.15) with *periodic boundary conditions*. The extension to more general cases can be done similarly. Note that the

matrix associated with the second order derivatives in (2.25) has one positive eigenvalue and one zero eigenvalue. This is not surprising since our moving mesh system is of parabolic type in the normal direction ($\mathbf{n}$) and of hyperbolic type in the tangential direction ($\mathbf{s}$). In fact, with these facts in mind, we can prove rigorously that the system (2.25) is well-posed.

We introduce the following Fourier transform for a periodic function g

$$\hat{g}(k) = \frac{1}{2\pi}\int_0^{2\pi} g(\alpha)e^{-ik\alpha}d\alpha$$

whose inverse is given by

$$g(\alpha) = \int \hat{g}(k)e^{ik\alpha}dk.$$

We consider the nonlinear parabolic equation

$$u_t + f(u)_x = \epsilon u_{xx} \tag{3.1}$$

with periodic boundary condition. Similar to the derivations in the last section, the moving mesh method is described by

$$\mathbf{X}_t = (x_t, \tilde{u}_t) = U\mathbf{n} + T\mathbf{s}, \tag{3.2}$$

where

$$U = -f'(\tilde{u})\sin\theta + \frac{\epsilon\kappa}{\cos^2\theta}, \qquad T = \mathtt{Int}\Big(\theta_\alpha U - < \theta_\alpha U >\Big). \tag{3.3}$$

Here $\mathtt{Int}$ is a pseudo-spectral integral operator defined in Fourier space by, for any 2π-periodic function g with mean zero

$$\widehat{\mathtt{Int}(g)}(k) = \begin{cases} (ik)^{-1}\hat{g}(k) & \text{for} \quad k \neq 0, \\ 0 & \text{for} \quad k = 0. \end{cases}$$

For a given function ρ defined in $[0, 2\pi]$, the mean is defined by

$$< \rho >= \frac{1}{2\pi}\int_0^{2\pi} \rho(\alpha)d\alpha.$$

Let $x(\alpha, t), \tilde{u}(\alpha, t)$ be a smooth, time dependent solution of the moving mesh equation (3.2). Denote by δx and $\delta\tilde{u}$ the perturbation in x and $\tilde{u}$ respectively. Similar assumptions are made for U, T etc. We perform first order perturbation by replacing $x, \tilde{u}$ in (3.2) by $x + \delta x, \tilde{u} + \delta\tilde{u}$. To prove the well-posedness of linearized motion, we will show that the perturbed quantities are bounded in some appropriate Sobolev norm.

It is useful to project $\mathbf{X}$ onto the normal and tangential directions. So we define

$$\delta\mathbf{X}^{\mathbf{n}} = (\delta x, \delta\tilde{u}) \cdot \mathbf{n}, \qquad \delta\mathbf{X}^{\mathbf{s}} = (\delta x, \delta\tilde{u}) \cdot \mathbf{s}.$$

The following results give the governing equations for the perturbations $\delta\mathbf{X}^{\mathbf{n}}$ and $\delta\mathbf{X}^{\mathbf{s}}$.

Lemma 3.1. *The linearized equations of the moving mesh system* (3.2) *for the nonlinear parabolic equation* (3.1) *satisfy*

$$\delta\mathbf{X}_t^{\mathbf{n}} = \frac{\epsilon}{\sigma^2\cos^2\theta}\delta\mathbf{X}_{\alpha\alpha}^{\mathbf{n}} + \tilde{g}(\theta, \sigma)\delta\mathbf{X}_\alpha^{\mathbf{n}} + A_0(\delta\mathbf{X}), \qquad \delta\mathbf{X}_t^{\mathbf{s}} = \frac{\epsilon\theta_\alpha}{\sigma^2\cos^2\theta}\delta\mathbf{X}_\alpha^{\mathbf{n}} + A_0(\delta\mathbf{X}) \tag{3.4}$$

where A_0 is some bounded operator, and

$$\tilde{g}(\theta, \sigma) = \frac{1}{\sigma}\left(-f'(\tilde{u})\cos\theta + \frac{2\epsilon\kappa\sin\theta}{\cos^3\theta}\right) + \frac{T}{\sigma}.$$

Proof. It follows from the moving mesh equations (3.2) and the definitions of $\delta\mathbf{X}^{\mathbf{n}}, \delta\mathbf{X}^{\mathbf{s}}$ that

$$\delta\mathbf{X}^{\mathbf{n}}_t = \delta U + \frac{T}{\sigma}\delta\mathbf{X}^{\mathbf{n}}_\alpha + A_0(\delta\mathbf{X}), \qquad \delta\mathbf{X}^{\mathbf{s}}_t = -\frac{U}{\sigma}\delta\mathbf{X}^{\mathbf{n}}_\alpha + \delta T + A_0(\delta\mathbf{X}) \tag{3.5}$$

where A_0 is a bounded operator. Furthermore, it can be shown that the linear part of $\delta\kappa$ has the following simple expression in terms of the normal component of $\delta\mathbf{X}$, see [3]

$$\delta\kappa = \frac{1}{\sigma}\left(\frac{1}{\sigma}\delta\mathbf{X}^{\mathbf{n}}_\alpha\right)_\alpha + A_0(\delta\mathbf{X}). \tag{3.6}$$

Similarly, the following result for $\delta\theta$ can be established

$$\delta\theta = \frac{1}{\sigma}\delta\mathbf{X}^{\mathbf{n}}_\alpha + A_0(\delta\mathbf{X}). \tag{3.7}$$

The above results, together with (3.3), lead to

$$\delta U = \frac{\epsilon}{\sigma^2\cos^2\theta}\delta\mathbf{X}^{\mathbf{n}}_{\alpha\alpha} + g(\theta,\sigma)\delta\mathbf{X}^{\mathbf{n}}_\alpha + A_0(\delta\mathbf{X}) \tag{3.8}$$

where

$$g(\theta,\sigma) = \frac{1}{\sigma}\left(-f'(\tilde{u})\cos\theta + \frac{2\epsilon\kappa\sin\theta}{\cos^3\theta}\right).$$

Combining (3.7) and (3.8) gives

$$\begin{aligned}\delta T &= \mathtt{Int}\Big(\delta\theta_\alpha U + \theta_\alpha\delta U - <\delta\theta_\alpha U + \theta_\alpha\delta U>\Big)\\ &= \frac{U}{\sigma}\delta\mathbf{X}^{\mathbf{n}}_{\alpha\alpha} + \frac{\epsilon\theta_\alpha}{\sigma^2\cos^2\theta}\delta\mathbf{X}^{\mathbf{n}}_\alpha + A_0(\delta\mathbf{X})\end{aligned} \tag{3.9}$$

The desired results then follow from (3.5) and (3.8)-(3.9).

Having Lemma 3.1, we are now ready to establish the linear well-posedness by using the energy methods.

Theorem 3.1. *(**Linear Wellposedness**) Let* $\mathbf{X}$ *be the smooth solution of the moving mesh equations (3.2)-(3.3). Then for* $0 \le t \le T$*, there exists a constant* M *such that the first order perturbation of* $\mathbf{X}$ *satisfies*

$$\|\delta\mathbf{X}(\cdot,t)\|_2 \le M\|\delta\mathbf{X}(\cdot,0)\|_2\,. \tag{3.10}$$

Proof. We will derive energy estimates for the leading order terms for $\delta\mathbf{X}^{\mathbf{n}}$ and $\delta\mathbf{X}^{\mathbf{s}}$. Multiplying $\delta\mathbf{X}^{\mathbf{n}}$ on both sides of (3.4) and integrating the resulting equation with respect to α yield

$$\begin{aligned}\frac{1}{2}\frac{d}{dt}\Big(\delta\mathbf{X}^{\mathbf{n}},\delta\mathbf{X}^{\mathbf{n}}\Big) &= \Big(\frac{\epsilon}{\sigma^2\cos^2\theta}\delta\mathbf{X}^{\mathbf{n}}_{\alpha\alpha},\delta\mathbf{X}^{\mathbf{n}}\Big) + \Big(\tilde{g}(\theta,\sigma)\delta\mathbf{X}^{\mathbf{n}}_\alpha,\delta\mathbf{X}^{\mathbf{n}}\Big) + e_1\\ &= -\Big(\frac{\epsilon}{\sigma^2\cos^2\theta}\delta\mathbf{X}^{\mathbf{n}}_\alpha,\delta\mathbf{X}^{\mathbf{n}}_\alpha\Big) + \Big(g_1(\theta,\sigma)\delta\mathbf{X}^{\mathbf{n}}_\alpha,\delta\mathbf{X}^{\mathbf{n}}\Big) + e_1,\end{aligned} \tag{3.11}$$

where the e_1 term is upper bounded by $|e_1| \le \|\delta\mathbf{X}\|_2^2$ and

$$g_1(\theta,\sigma) = \tilde{g}(\theta,\sigma) - \Big(\frac{\epsilon}{\sigma^2\cos^2\theta}\Big)_\alpha\,.$$

It follows from the integration by parts that

$$\Big(g_1(\theta,\sigma)\delta\mathbf{X}^{\mathbf{n}}_{\alpha},\delta\mathbf{X}^{\mathbf{n}}\Big)=-\Big(g_1(\theta,\sigma)\delta\mathbf{X}^{\mathbf{n}}_{\alpha},\delta\mathbf{X}^{\mathbf{n}}\Big)-\Big((g_1)_{\alpha}(\theta,\sigma)\delta\mathbf{X}^{\mathbf{n}},\delta\mathbf{X}^{\mathbf{n}}\Big)$$

and so we have

$$\Big(g_1(\theta,\sigma)\delta\mathbf{X}^{\mathbf{n}}_{\alpha},\delta\mathbf{X}^{\mathbf{n}}\Big)\le C\|\delta\mathbf{X}\|_2^2\,. \tag{3.12}$$

Multiplying $\delta\mathbf{X}^{\mathbf{s}}$ to the $\delta\mathbf{X}^{\mathbf{s}}$ equation and integrating the resulting equation with respect to α, we obtain

$$\begin{aligned}\frac{1}{2}\frac{d}{dt}(\delta\mathbf{X}^{\mathbf{s}},\delta\mathbf{X}^{\mathbf{s}}) &= \Big(\frac{\epsilon\theta_{\alpha}}{\sigma^2\cos^2\theta}\delta\mathbf{X}^{\mathbf{n}}_{\alpha},\delta\mathbf{X}^{\mathbf{s}}\Big)+e_2\\ &\le \frac{1}{2}\Big(\frac{\epsilon}{\sigma^2\cos^2\theta}\delta\mathbf{X}^{\mathbf{n}}_{\alpha},\delta\mathbf{X}^{\mathbf{n}}_{\alpha}\Big)+e_3\end{aligned} \tag{3.13}$$

where the terms e_2 and e_3 are upper bounded by $\|\delta\mathbf{X}^{\mathbf{n}}\|_2^2+\|\delta\mathbf{X}^{\mathbf{s}}\|_2^2$. Combining (3.11)-(3.13), we obtain

$$\frac{d}{dt}\Big((\delta\mathbf{X}^{\mathbf{n}},\delta\mathbf{X}^{\mathbf{n}})+(\delta\mathbf{X}^{\mathbf{s}},\delta\mathbf{X}^{\mathbf{s}})\Big)\le C\Big((\delta\mathbf{X}^{\mathbf{n}},\delta\mathbf{X}^{\mathbf{n}})+(\delta\mathbf{X}^{\mathbf{s}},\delta\mathbf{X}^{\mathbf{s}})\Big)\,. \tag{3.14}$$

The estimate (3.10) now follows from the standard results of the Gronwall inequality.

Remark 1. The constant M in (3.10) depend not only on T, but also on the viscosity coefficient ϵ. It will be interesting to see how to modify our adaptive grid method so that M is independent (or weakly dependent) on ϵ.

4. Numerical Methods

In this section, discrete methods for solving the DAEs derived in Section 2 will be discussed. For simplicity, we consider the viscous conservation laws only. The ideas used in this section can be extended to deal with the Heat equation and the KdV equation in a straightforward way. We begin by considering how to obtain initial data for $\theta, L, \tilde{u}$ etc. We assume that $u(x,0)=v(x)$ is given.

- `Step 1:` Compute the initial arclength by using the definition

$$L(0)=\int_a^b\sqrt{1+v_x^2(x)}dx.$$

- `Step 2:` Compute $x(\alpha,0)$ by using the following ODE and the 4th-order Runge-Kutta method

$$x_{\alpha}=\frac{L(0)}{\sqrt{1+v_x^2(x)}},\qquad x(0,0)=a.$$

  For very stiff initial data, the following strategy should be employed to select the initial grid:

$$\int_{x(\alpha_j,0)}^{x(\alpha_{j+1},0)}\sqrt{1+u_x^2}dx=\frac{L(0)}{N}.$$

- `Step 3:` Compute $\tilde{u}(\alpha,0)$ via $\tilde{u}(\alpha,0)=v(x(\alpha,0))$.

- `Step 4:` Compute $\theta(\alpha,0)$ via $\theta(\alpha,0)=\tan^{-1}\left(v_x(x(\alpha,0))\right)$.

- Step 5: Determine $U(\alpha,0)$ by using (2.17)

$$U(\alpha,0) = -f'(\tilde{u}(\alpha,0))\sin\theta(\alpha,0) + \epsilon v_{xx}(x(\alpha,0))\cos\theta(\alpha,0)\,.$$

- Step 6: Evaluate $T(\alpha,0)$ using the repeated Simpson's rule.

Spatial discretization. We discretize the first and second derivatives in α by using the three-point central finite-differences. For third derivatives, the standard five-point central differences are employed.

Temporal discretization. Assume for now that space is continuous. We only discuss the $-\tilde{u}$ formulation for the viscous conversation laws. Let $\mathbf{U} = [x(\alpha_1,t), \tilde{u}(\alpha_1,t), \cdots, x(\alpha_{N-1},t), \tilde{u}(\alpha_{N-1},t)]^T$. Then the governing equations for x and $\tilde{u}$ can be written in the following vector form:

$$\mathbf{U}_t = \mathbf{F}\big(\mathbf{U}_{\alpha\alpha}, \mathbf{U}, \theta, \mathbf{L}, \mathbf{T}\big)\,.$$

The discretization scheme for time is the following (implicit) Crank-Nicholson method:

$$\mathbf{U}^{n+1} = \mathbf{U}^n + \frac{\Delta t}{2}\Big(\mathbf{F}\big(\mathbf{U}^{n+1}_{\alpha\alpha}, \mathbf{U}^{n+1}, \theta^{n+1}, L^{n+1}, T^{n+1}\big) + \mathbf{F}\big(\mathbf{U}^{n}_{\alpha\alpha}, \mathbf{U}^{n}, \theta^{n}, L^{n}, T^{n}\big)\Big).$$

This procedure requires 3 to 5 simple iterations at each time step.

Numerical Integration. To evaluate the tangential velocity $T(\alpha,t)$, we need to use the repeated Simpson's rule. However, this rule can be applied only when the number of the grid point is even. For odd number some adjustment has to be made. One way is to apply the so-called *three-eight rule* over four adjacent points and the Simpson's rule over the rest of the interval. In our computation, we use the three-eights rule at the upper end. This method is called Simpson's method II, see p. 99 of [11].

5. Numerical Experiments

Here we carry out some numerical experiments to examine the proposed moving mesh methods. We choose three examples, consisting of two parabolic equations and one KdV equation. Particular attention will be given to Example 5.2, since this problem is often used as a test (occasionally the only test) of mesh selection strategies.

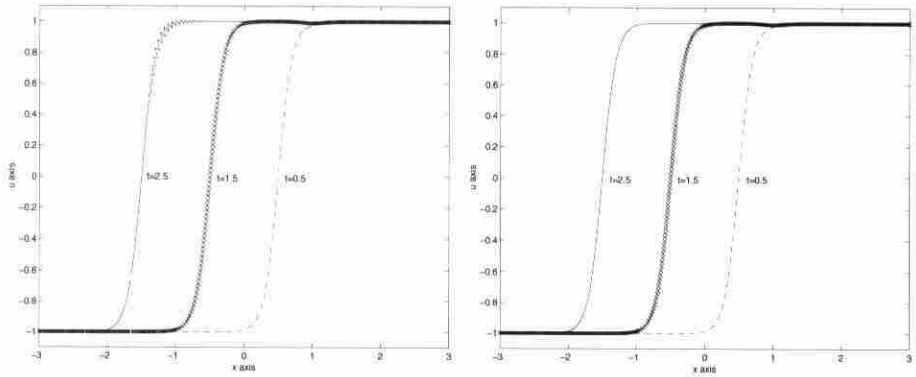

Fig1. The solutions to the Heat equation with $\epsilon = 10^{-4}, t = 0.5, 1.5, 2$ and 2.5. left: $N = 240, \Delta t = N^{-1}$; right: $N = 270, \Delta t = N^{-1}$.

Example 5.1. The first example is a Heat conduction problem

$$u_t = \epsilon u_{xx} + S(x,t) \qquad -3 < x < 3,\ t > 0$$

where the initial conditions, Dirichlet boundary conditions and source term S are chosen such that the exact solution is

$$u(x,t) = \tanh\Big(r_1(x-1) + r_2 t\Big), \qquad -3 \le x \le 3,\ t > 0.$$

Coyle, Flaherty and Ludwig studied this problem [6]. The above solution travels in the negative x direction when the constants r_1 and r_2 are positive. We solve this problem for $r_1 = r_2 = 5$ and $\epsilon = 10^{-4}$, and show the results at $t = 0.1, 0.5, 1$ and 1.5 in Figure 1.

We first use 240 points in the computation (40 points in each unit interval). The left graph in Figure 1 shows that computed solutions are satisfactory for $t \le 1.5$, but they become oscillating when $t = 2.5$, which is due to the (simple) second-order central difference methods used in the computations. Theorem 3.1 ensures that the present moving mesh method is well-posed. It suggests that for a fixed ϵ larger N will produce more accurate numerical results and there will have no numerical instability. To see this, we add 5 more points in each unit interval and as a result the oscillations are eliminated, see Figure 1.

Example 5.2. The second example is the well-known Burgers' equation

$$\begin{aligned} &u_t + uu_x = \epsilon u_{xx}\,, \qquad 0 < x < 1, \quad t > 0 \\ &u(0,t) = u(1,t) = 0\,, \qquad t > 0 \\ &u(x,0) = \sin(2\pi x) + 0.5 * \sin(\pi x)\,. \qquad 0 \le x \le 1 \end{aligned}$$

As time increases, the sinusoidal initial condition first steepens to a near-shock and then propagates to the right boundary while simultaneously damping. Figure 2 shows numerical solutions with $N = 80$. On the left, we plot the solution profile at $t = 0.1, 0.5, 0.8, 1.3$. They are in good agreement with the existing results, see e.g. [16, 18]. On the right side of the figure, we use circles to denote the location of the numerical solutions, $(x(\alpha_j,t), \tilde{u}(\alpha_j,t))$. It seems surprising that the initial distribution does not satisfy the equal-arclength requirement. However, by observing that the ratio of the scales in x and y-axis is $1 : 2.3$ and also by checking the values of the local arc-length derivative σ, we conclude that the equal-arclength requirement is indeed satisfied for the initial distribution.

Again, to show that the numerical method is stable we double the number of points used in the spatial direction. Namely, we use $N = 160$ to solve Example 5.2. The numerical results are shown in Figure 3. It is seen that smoother numerical solutions are obtained with $N = 160$, especially when $t = 0.5$.

We now change the perturbation parameter ϵ to 10^{-4}. This implies that a very small viscosity is involved in this problem. Indeed, at a finite time, a sharp layer with large gradient (almost a shock) is developed with this small viscosity. Our numerical experiments with $N = 80$ and $N = 160$ indicate that sharp layer is developed at $t \approx 0.17$, see Figure 5. In this case, we observe that many numerical points are clustered near $x \approx 0.58$ and near this value of x the value of tangent angle θ is approximately $-\pi/2$. Since $|\theta| \approx \pi/2$, the evaluation of the normal velocity U becomes extremely difficult due to last term in the formula (2.17). Therefore, one of the limitations of our moving grid method is that numerical solutions cannot be obtained after a shock is (almost) formed.

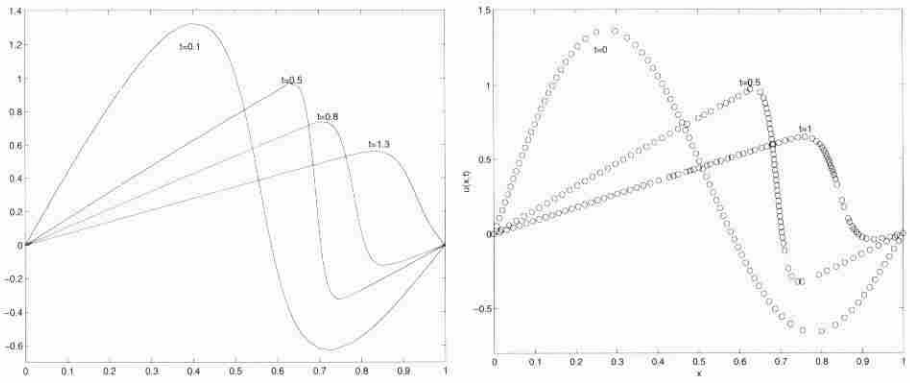

Fig 2. Burgers' equation with $\epsilon = 10^{-2}, N = 80, \Delta t = 0.1N^{-1}$. left: $t = 0.2, 0.5, 0.8, 1.3$; right: $t = 0, 0.5, 1$.

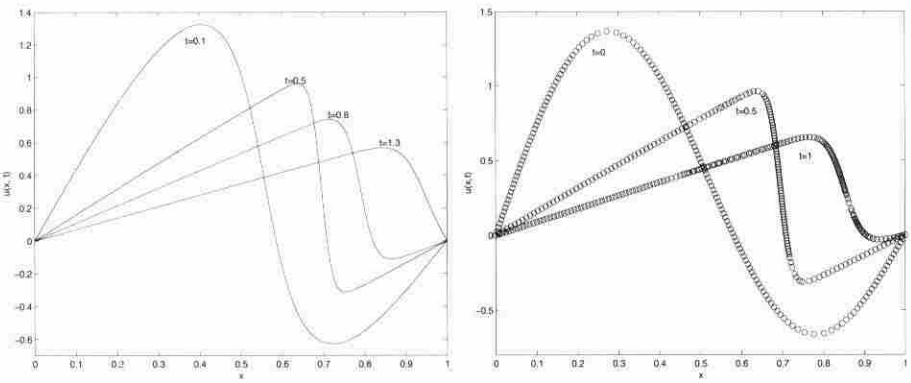

Fig 3. Same as Figure , except $N = 160$.

We further look at the (moving) grid distribution against the variable α, which is the independent variable in the computational space. In Figure 6 we plot $x(\alpha, t)$ at $t = 0.17$ as a function of α. It is seen that more points in the physical space cluster in the region where a sharp layer is formed.

Example 5.3. The third example is a KdV equation

$$u_t + \beta u u_x + \mu u_{xxx} = 0, \qquad x \in [-p, p] \tag{5.1}$$

where β and μ are given constants.

Some *linear* properties for solutions of (2.18) were observed numerically by Zabusky and Kruskel in 1965. The soliton theory has been established based on the numerical study of the KdV equation. One of the exact solutions for the equation (2.18) is

$$u(x,t) = \frac{3c}{\beta}\text{sech}^2\left(\frac{1}{2}\sqrt{\frac{c}{\mu}}(x - ct - x_0)\right), \tag{5.2}$$

where c and x_0 are some constants.

We choose $x_0 = 0, c = 2, \mu = 2$ and $\beta = 6$ as our test problem. The solution domain is $(-15, 15)$. In Figure 7, we plot the exact solution and numerical solutions at $t = 1$ with $N = 64$,

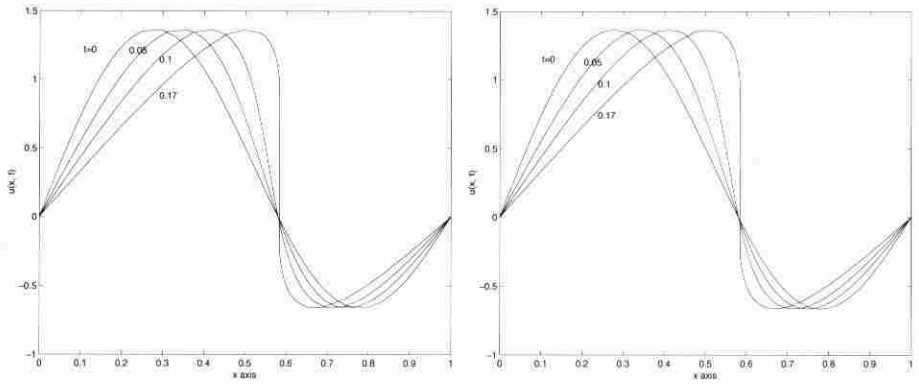

Fig 4. Burgers' equation with $\epsilon = 10^{-4}, N = 80, \Delta t = 0.1N^{-1}$ at $t = 0, 0.05, 0.1, 0.17$. left: $N = 80$; right: $N = 160$.

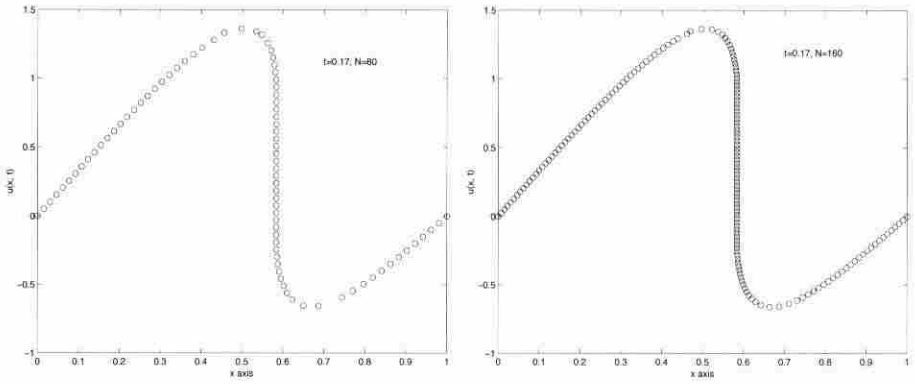

Fig 5. Burgers' equation with $\epsilon = 10^{-4}, \Delta t = 0.1N^{-1}$ and $t = 0.17$. left: $N = 80$; right: $N = 160$.

respectively. To see the accuracy of the moving mesh solutions, we also compute the Equation (5.1) using Fornberg and Whitham's spectral code [8]. Below we will briefly describe Fornberg and Whitham's approach. A simple change of variable ($x \to \pi x/p + \pi$) changes the solution interval $[-p,\ p]$ to $[0, 2\pi]$. The equation (5.1) becomes

$$u_t + \frac{\beta\pi}{p} u u_x + \frac{\mu\pi^3}{p^3} u_{xxx} = 0, \qquad x \in [0, 2\pi]. \tag{5.3}$$

It is known that

$$\frac{\partial^n u}{\partial x^n} = \mathcal{F}^{-1}\{(ik)^n \mathcal{F}\{u\}\}, \qquad n = 1, 2, \cdots$$

where $\mathcal{F}$ and $\mathcal{F}^{-1}$ are the Fourier and the inverse Fourier transform operators, respectively. An application of the above results (with $n = 1$ and 3) to (5.3) gives

$$\frac{du(x_j, t)}{dt} = -\frac{i\beta\pi}{p} u(x_j, t) F^{-1}(kF(u)) + \frac{i\mu\pi^3}{p^3} F^{-1}(k^3 F(u)), \qquad 1 \le j \le N - 1 \tag{5.4}$$

where the continuous Fourier transforms were replaced by the discrete transforms F and F^{-1}. Fornberg and Whitham used two-step time discretization and FFT algorithms to solve the equation (5.4). Figure 7 also includes numerical solutions at $t = 1$ computed by the spectral methods with $N = 64$. Graphically the moving mesh solutions and the spectral solutions are

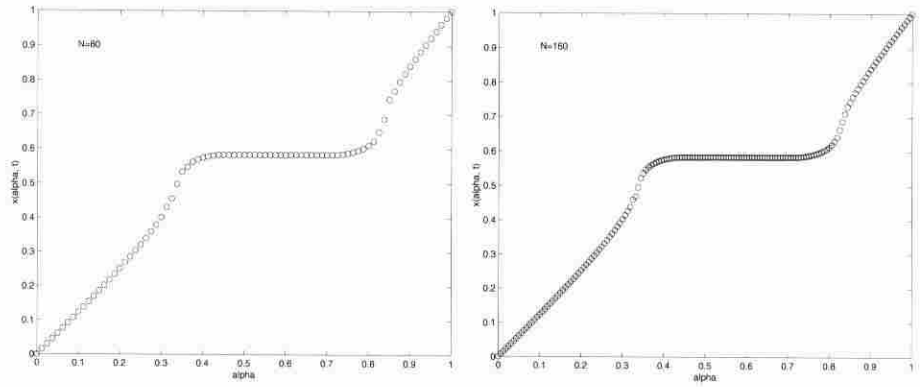

Fig 6. $x(\alpha, t)$ at $t = 0.17$ as a function of α.

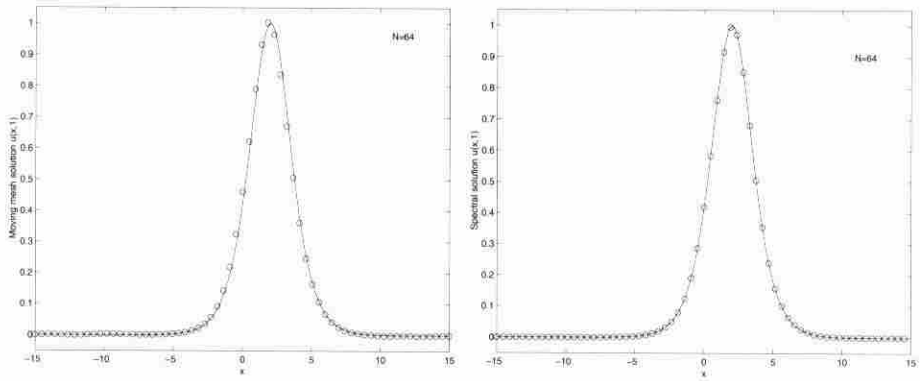

Fig 7. KdV equation with $\mu = 2$ and $\beta = 6$. The circle denote the numerical solution and the solid line is the exact solution. left: moving grid solution; right: Fornberg and Whitman's spectral solution.

comparable with each other, although the maximum error with the moving mesh methods is slightly greater than that obtained by using the spectral methods.

References

[1] S. Adjerid, J.E. Flaherty, A moving fem with error estimation and refinement for 1-d time dependent pdes. *SIAM J. Numer. Anal.*, **23** (1986), 778–795.

[2] D.A. Anderson, Adaptive mesh schemes based on grid speeds, *AIAA Paper*, **83**:1931 (1983), 311.

[3] J.T. Beale, T.Y. Hou, J. Lowengrub, Growth rates for the linear motion of fluid interfaces away from equilibrium, *Comm. Pure Appl. Math.*, **46** (1993), 1269–1301.

[4] N. Carlson, K. Miller, Design and application of a gradient-weighted moving finite code, part i, in 1-d, *SIAM J. Sci. Comput.*, **19** (1998), 728–765.

[5] N. Carlson, K. Miller, Design and application of a gradient-weighted moving finite code, part ii, 2-d, *SIAM J. Sci. Comput.*, **19** (1998), 766–798.

[6] J. Coyle, J. Flaherty, R. Ludwig, On the stability of mesh equidistributing strategies for time dependent pdes, *J. Comput, Phys.*, **62** (1986), 26–39.

[7] C. de Boor, Good approximation by splines with variable knots ii, Springer Lecture Notes Series 363, Springer Verlag, Berlin, 1973.

[8] B. Fornberg, G.B. Whitham, A numerical and theoretical study of certain nonlinear wave phenomena, *Phil. Trans. Royal Soc. London*, **289** (1978), 373–404.

[9] R.G. Hindman, J. Spencer, A new approach to truely adaptive grid generation, *AIAA Paper*, **83**:0450 (1983), 1.

[10] T.Y. Hou, J.S. Lowengrub, M.J. Shelley, Removing the stiffness from interfacial flows with surface tension, *J. Comput. Phys.*, **114** (1994), 312–338.

[11] P. Linz, Analytical and Numerical Methods for Volterra Equations, SIAM, Philadelphia, 1985.

[12] K. Miller, Moving finite element methods ii, *SIAM J. Numer. Anal.*, **18** (1981), 1033–1057.

[13] K. Miller, A geometrical-mechanical interpolation of gradient-weighted moving finite elements, *SIAM J. Numer. Anal.*, **34** (1997), 67–90.

[14] K. Miller, R.N. Miller, Moving finite element methods I, *SIAM J. Numer. Anal.*, **18** (1981), 1019–1032.

[15] Y. Qiu, D.M. Sloan, T. Tang, Numerical solution of a singularly perturbed two-point boundary value problem using equidistribution: analysis of convergence, *J. Comput. Appl. Math.* **116** (2000), 121–143.

[16] Y. Ren, Theory and Computation of Moving Mesh Methods for Solving Time-Dependent Partial Differential Equations, PhD thesis, Simon Fraser University, B.C., Canada, 1991.

[17] W.Z. Huang, Y. Ren, R.D. Russell, Moving mesh partial differential equations (mmpdes) based on the equidistribution principle, *SIAM J. Numer. Anal.*, **31** (1994), 709–730.

[18] P.A. Zegeling, J.G. Blom, An evaluation of the gradient-weighted moving-finite-element method in one space dimension, *J. Comput. Phys.*, **103** (1992), 442–441.